

Analysis of Slip Flow in Microchannels

Derek C. Tretheway⁽¹⁾, Xiaojun Liu, and Carl D. Meinhart⁽²⁾

Department of Mechanical Engineering
University of California
Santa Barbara, CA 93106

⁽¹⁾ e-mail: tretdec@engineering.ucsb.edu

⁽²⁾ e-mail: meinhart@engineering.ucsb.edu

ABSTRACT

Since the surface to volume ratio in enclosed flow devices scales as L^{-1} , the small length scale associated with micro-devices dictates the importance of boundary conditions. Several researchers have suggested that the well-accepted no-slip boundary condition may not be suitable for flows at the micro- and nano-scale (Zhu and Granik, 2001; Ruckenstein & Rajora, 1983; Barrat & Bocquet, 2000; Craig et. al., 2001; Tretheway and Meinhart, 2002). The current work addresses the controversy of fluid slip and proposes a mechanism for the apparent slip at a hydrophobic surface. With micron-resolution Particle Image Velocimetry (μ -PIV) we measure the flow of water in 30 x 300 micron channels. The spatial resolution of the μ -PIV measurements is defined by the size of the interrogation window to be 14.7 x 0.9 x 1.8 microns with velocity measurements obtained to within 450nm of the channel wall. The measured velocity profile for flow near the wall of a hydrophilic microchannel is consistent with the theoretical profile assuming no-slip. Figure A1 shows the velocity profile for flow near the wall of an OTS-coated, hydrophobic microchannel. The velocity profile exhibits significant deviations from the no-slip condition with a slip velocity of approximately 10% the free stream velocity. This slip velocity yields a slip length equal to 0.92 microns. These results indicate that the no-slip condition is not necessarily valid for hydrophilic liquids flowing over hydrophobic boundaries. Recently, Tyrrell and Attard (2001) observed the presence of nanobubbles on a hydrophobic surface submerged in water. In order to determine the effect nanobubbles may have on fluid flow, we solve Stokes flow between two infinite parallel plates with the nanobubbles modeled as a thin, one-dimensional air gap at the surface. Figure A2 shows the air gap required to yield a given slip length for various plate separations. For the measured slip length of 0.92 microns, an air gap of approximately 18nm would be required. This bubble height is consistent with the measured bubble heights of Tyrrell and Attard (2001). Therefore, the measured apparent fluid slip may develop from the presence of nanobubbles on the hydrophobic surface.

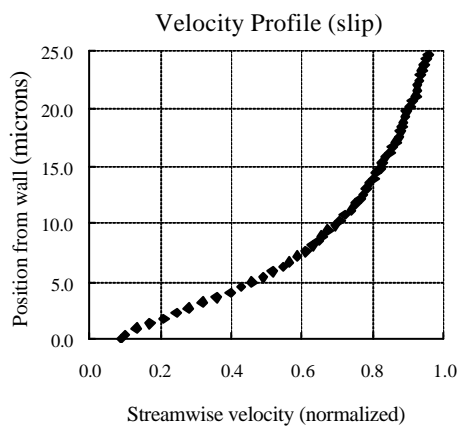


Figure A1. Velocity profile for water flowing through an OTS, hydrophobic microchannel. (slip)

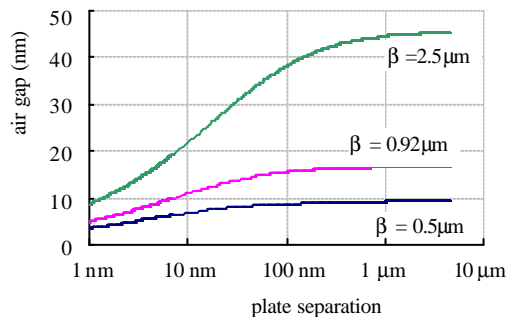


Figure A2. Required air gap thickness as a function of plate separation to produce a given slip length.

1. INTRODUCTION

For almost a hundred years scientists and engineers have applied the no-slip boundary condition to fluid flow over a solid surface. While the well accepted no-slip boundary condition has been validated experimentally for a number of macroscopic flows, it remains an assumption not based on physical principles. In fact, nearly two hundred years ago Navier (1823) proposed a more general boundary condition, which includes the possibility of fluid slip. Navier's proposed boundary condition assumes that the velocity, v_x , at a solid surface is proportional to the shear rate at the surface

$$v_x = \beta (dv_x/dy), \quad (1)$$

where β is the slip length or slip coefficient. If $\beta=0$ then the generally assumed no-slip boundary condition is obtained. If β is finite, fluid slip occurs at the wall, but its effect depends upon the length scale of the flow. For example, the solution for Stokes flow between two infinite parallel plates with the boundary conditions of no shear stress at the centerline and Navier's hypothesis (1) at the wall, yields

$$v_x = \frac{h^2}{2\mu} \left(-\frac{dp}{dx} \right) \left[\left(1 - \left(\frac{y}{h} \right)^2 \right) + \frac{2\beta}{h} \right], \quad (2)$$

where $2h$ is the distance between the two plates, μ is the viscosity, and $(-dp/dx)$ is the pressure drop. The first term in the brackets, $1-(y/h)^2$, is the standard solution for pressure-driven Stokes flow between two infinite parallel plates with no-slip, while the second term, $2\beta/h$, represents an additional velocity associated with the general boundary condition (1). The first term is of order one while the second term depends on the plate separation, h . If β is finite, the importance of the second term increases as h decreases, and for a given β , there is a sufficiently small length scale at which this term not only becomes comparable to the first but dominates equation (2). Since the no-slip assumption appears to be valid at the macroscale, β must be relatively small for Navier's hypothesis to hold. However, it's not readily apparent that the second term in equation (2) will remain negligible for flows in microdevices where the characteristic length scale is on the order of microns.

Recently, several researchers have suggested that the well-accepted no-slip boundary condition may not be suitable at both the micro- and nano-scale. With a hot-wire anemometer Watanabe et.al. (1998, 1999) identify fluid slip at the wall of a strongly hydrophobic duct or pipe. Their velocity profiles are consistent with Navier's hypothesis. However, their results are for a relatively large-scale rectangular duct (15mm x 15mm) and modest Reynolds numbers. Ruckenstein and Rajora (1983) investigated fluid slip in glass capillaries with surfaces made repellent to the flowing liquid. Their experimental results of pressure drop indicate larger slip than that predicted by chemical potential theory, where slip is proportional to the gradient in the chemical potential. The results suggest that slip occurs over a gap near the surface rather than directly on the solid surface, and the gap forms when a hydrophobic liquid flows over a hydrophilic surface and vice versa. They suggest the gap may be increased in thickness by the release of gases entrained in the flowing liquid and/or the desorption of soluble gases. Their results, however, are inferred from pressure drop-flow measurements and not direct measurement of the fluid velocities. Computationally, Barrat and Bocquet (1999) expect significant slip in nanoporous medium when the liquid is sufficiently non-wetting, which increases the effective permeability of the nanoporous medium. Their predictions are experimentally justified by Churaev et. al. (1984) who postulated slip at the wall to recover the viscosity of water for water flow in thin ($<1\mu\text{m}$) hydrophobic capillaries. Pit et. al. (2000) observe fluid slip for hexadecane between two rotating parallel disks with a gap of 190 microns. By following the movement of a photo-bleached test section, they measure no slip when the surfaces are coated with perfluorodecanetrichlorosilane, a slip length of approximately 170nm for bare sapphire, and a slip length of 400nm for an octadecyltrichlorosilane (OTS) coating. They conclude that slip depends on both the interfacial energy and surface roughness. At a much smaller lengthscale, Craig et. al. (2001) calculate the drainage force for a sphere approaching a solid, flat wall. They measure slip lengths up to 20nm for aqueous sucrose solutions that have advancing and receding contact angles of 70 and 40 degrees respectively. They conclude that the slip length depends non-linearly on the approach rate of the sphere. Zhu and Granick (2001) experimentally observe fluid slip in an oscillating surface force apparatus. For cylinder separations from approximately 10-200nm, they measure slip lengths (point into the wall at which

the inferred velocity would go to zero) of up to $2.5\ \mu\text{m}$ for water between octadecyltriethoxysilane (OTE) surfaces, $1.5\ \mu\text{m}$ for tetradecane between OTE surfaces, and $0.9\ \mu\text{m}$ for tetradecane between mica surfaces. Their results suggest a strong dependence between the velocity gradient and magnitude of the slip, a critical shear rate for onset of fluid slip, and an increase in the slip length as the separation between the cylinders decreases. Their conclusions, however, are inferred from discrepancies between the measured normal force and expected normal force assuming no-slip, and are not measured directly. More recently, Zhu and Granick (2002) examine the relative importance of surface roughness and fluid-surface interactions in determining the appropriate boundary condition. For similar, poorly wetting surfaces the critical shear rate to observe deviations from force predictions assuming no-slip increased nearly exponentially with increasing surface roughness. They conclude that local intermolecular interactions are dominant when surfaces are very smooth, but are otherwise negligible at sufficient surface roughness. Tretheway and Meinhart (2002) measured fluid velocities in hydrophilic and hydrophobic microchannels by micron resolution particle image velocimetry (μ -PIV). Their results showed a significant fluid velocity near a hydrophobic microchannel wall and no-slip for a hydrophilic surface. A slip length of 0.92 microns was estimated.

In the current work, we analyze slip flows in microchannels, review the techniques and results of Tretheway and Meinhart (2002) and propose a mechanism for the apparent fluid slip in a hydrophobic channel.

2. Experimental System

Figure 1 is a schematic of the micro-PIV measurement system. The pulses of two frequency-doubled Nd:YAG lasers ($\lambda=532\ \text{nm}$) are combined, directed through a fiber optic cable, and expanded into the illumination port of a Nikon Eclipse TE200 inverted microscope. The pulses are reflected by an epi-fluorescent prism and relayed through a NA=1.4, 60X oil immersion objective lens into the microchannel. Fluorescently dyed 300nm diameter flow-tracing polystyrene spheres absorb the green ($\lambda=532$) laser light and emit red ($\lambda=575$) light. The fluorescent light is imaged by the objective lens and passed through the epi-fluorescent filter cube, where green light from background reflection is removed. The remaining red

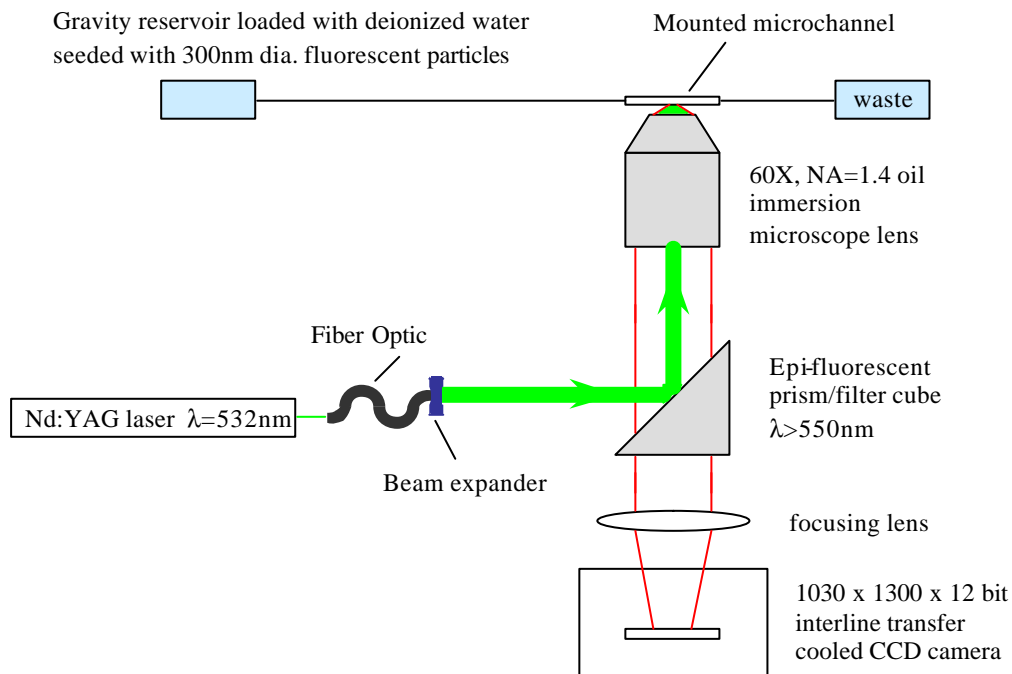


Figure 1. Experimental micro-particle image velocimetry (μ -PIV) setup.

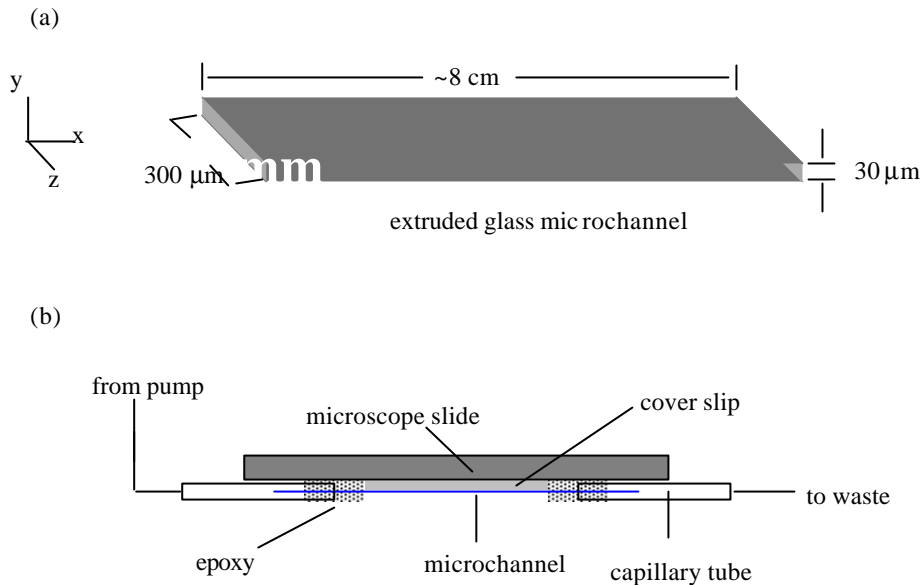


Figure 2. Schematic of the glass microchannel; a) dimensions of the microchannel are 30mm thick by 300mm wide by 8cm long. b) microchannel is mounted to a microscope slide and cover slip, inserted into capillary tubes, and sealed with epoxy.

light is focused by a relay lens onto a cooled 1030 x 1300 x 12 bit interline transfer CCD camera. A cooled CCD camera is required to suppress dark-current noise so that the low light levels emitted by the fluorescent particles can be recorded. The interline transfer feature allows back-to-back recording of two images with a minimum time delay of 500ns. The duration of a single laser light pulse combined with the decay time of the fluorescent dye is on the order of 5-10ns, which effectively freezes the motion of the particles. The delay time between the two laser pulses is 150µs. The two images captured by the CCD camera are then analyzed with PIV software developed by Steve Wereley (currently at the Dept. of Mechanical Engineering, Purdue University). The interrogation region is set at 128 x 8 pixels, which yields a spatial resolution of 14.7µm in the streamwise direction, 900nm in the spanwise direction and 1.8µm in depth. With a 50% overlap of interrogation regions, we obtain velocity measurements to within 450nm of the channel wall. To increase the signal to noise ratio, 48 image pairs are cross correlated and the resulting correlations ensemble averaged (Meinhart et.al., 2000).

We measure velocities in 30µm deep by 300µm wide extruded glass microchannels trimmed to a length of approximately 8cm (see Figure 2a). For measurement purposes, a microchannel is mounted on a microscope slide. A cover slip is inserted between the microchannel and microscope slide to displace the microchannel from the slide and provide rigid support. The ends of the microchannel are inserted into capillary tubes and sealed with an epoxy. The microscope slide (with the microchannel, cover slip, and capillary tubes attached) is then inverted and set into a bracket mounted to the translation stage directly above the objective lens (see Figure 2b). Deionized water seeded with the 300nm diameter fluorescent polystyrene spheres (Interfacial Dynamics Corporation) is injected through tubing attached to the capillary tube into the microchannel by a gravity feed system. The flow rate is constant at approximately 200µl/hr.

Measurements are taken in the mid plane of the channel (15µm from the bottom) near the side wall at a distance 4 to 4.5cm from the entrance of the microchannel. This ensures a fully developed flow profile. The field of view is aligned such that a section of the wall is included in each image. Since there are no particles in the wall, the resulting PIV correlations outside the region of flow produce erroneous velocity vectors with magnitudes and directions that are inconsistent with the known direction of flow. The wall location is determined as the position where the correlations for a given position become completely

random. This provides a more accurate location of the wall than can be achieved by visual inspection of the CCD camera images.

We compare the velocity profiles in hydrophilic and hydrophobic microchannels. An untreated glass microchannel is naturally hydrophilic. Hydrophobic microchannels are created by coating the walls of the microchannel with octadecyltrichlorosilane (OTS). The untreated microchannel is first pre-treated with a concentrated sodiumhydroxide solution, which opens the silicon oxide layer by creating hydroxyl groups. The microchannels are then rinsed with water and dried thoroughly. The cleaned microchannel is then exposed multiple times to a 2mM solution of OTS in dicyclohexyl for approximately one to two hours during each exposure. During this time, OTS reacts with the silicon atom of the exposed hydroxyl groups. The OTS reaction with silicon is autophobic, which limits the coating to a single monolayer. After the OTS exposure, the microchannels are rinsed with chloroform and dried. The microchannels are then baked at 100°C overnight. This curing process cross-links the individual OTS molecules creating a smooth and robust monolayer. At maximum density the OTS layer is approximately 23 angstroms thick with a surface roughness of 2-3 angstroms. As the contact angle cannot be measured inside the microchannel, a reference section of glass is treated concurrently with the microchannels to provide an estimate of the effectiveness of the reaction. We measure contact angles for water of approximately 120°, which is consistent with previously measured contact angles of OTS.

3. Results

Figure 3 shows the average velocity profile for flow near the wall of a hydrophilic microchannel. The velocity is normalized with the free-stream velocity. The velocity is near its free-stream value at 25 microns and smoothly decreases to zero near the wall. The velocity profile is consistent with the analytical solution for flow through a rectangular channel with a finite aspect ratio, which indicates that at this length scale the no-slip boundary condition is valid for water flowing over a hydrophilic surface.

Figure 4 shows the average velocity profile for the flow of a hydrophilic liquid (deionized water) near the wall of a hydrophobic, OTS coated microchannel. If the no-slip boundary condition were valid, we would expect the velocity profile to smoothly approach zero at the boundary. The results displayed in Fig. 4 exhibit significant deviations from the profiles displayed in Fig. 3. While the velocity is a maximum in the center of the channel and decreases towards the boundary, a finite and significant velocity is measured at the location of the hydrophobic wall. From the measured shear rate at the wall, we calculate a slip length equal to 0.92 microns. This slip length is consistent with the measured slip lengths of Zhu and Granick (2001) and Pit et. al. (2000).

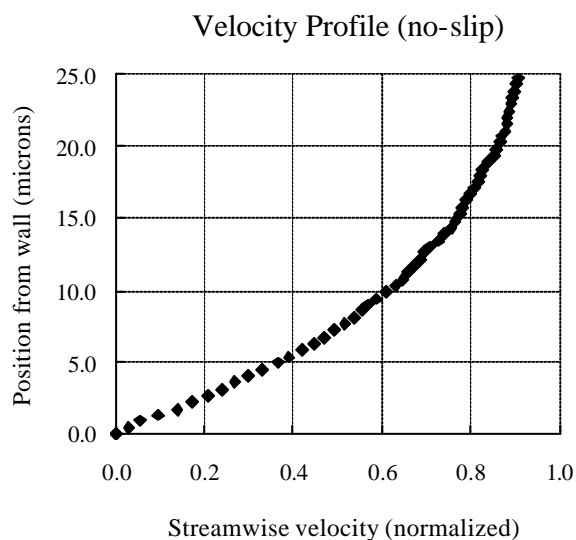


Figure 3. Velocity profile for water flowing through a clean, hydrophilic microchannel. (no-slip)

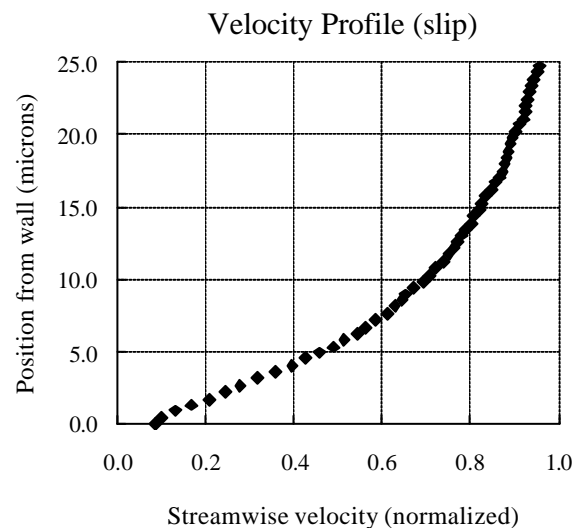


Figure 4. Velocity profile for water flowing through an OTS, hydrophobic microchannel. (slip)

4. Discussion

The mechanism for the generation of apparent fluid slip is unknown. Ruckenstein and Rajora (1983) suggest that fluid slip may develop from entrained and soluble gases forming a gap near the wall. Recently, Tyrell and Attard (2001) imaged, with an atomic force microscope, a hydrophobic glass surface submerged in water. Their results showed the presence of pancake shaped, 20 to 30 nm thick nano-bubbles completely covering the surface. In addition, they showed that the hydrophobic surface acts as a nucleation site pulling dissolved gasses out of solution. Within 10 to 20 minutes after scraping the surface clean, the surface was once again completely covered with nano-bubbles.

In this work, velocity measurements were made for deionized water flowing over a hydrophobic surface. No treatment of the water was conducted to remove dissolved or entrained gasses. To determine if dissolved gasses could generate the apparent fluid slip in Fig. 4, we examine analytically flow between two infinite parallel plates assuming nano-bubbles form an effective air gap near the wall. From this simple one dimensional model we can calculate the bubble height or air gap required to generate measured slip lengths assuming Navier's hypothesis effectively describes a thin air gap at the surface. For two phase flow between two infinite parallel plates with a thin air gap of thickness, δ , at the wall and a fluid layer of thickness $2h$, the solution for the velocity in the water phase assuming Stokes flow for both phases, no stress at the centerline, continuity of stress and velocity at the air-water interface, and no-slip at the air-wall interface is

$$u_w = \frac{1}{2\mu_w} \left(\frac{dP}{dx} \right)_w \left[y^2 - 2hy - 2 \frac{\mu_w}{\mu_a} h d - \frac{\mu_w}{\mu_a} d^2 \right], \quad (3)$$

where μ_a and μ_w are the viscosity of air and water respectively, $(-dp/dx)$ is the pressure drop and $y=0$ at the air water interface. Assuming Navier's hypothesis effectively describes the thin air gap at the wall we set the velocity equal to the slip length times the shear rate and obtain an equation for the air gap thickness (or bubble height) as a function of plate separation and slip length

$$\frac{d^2}{2} + hd - \frac{\mu_a}{\mu_w} \beta h = 0. \quad (4)$$

Figure 5 shows the air gap thickness required for a given plate separation to generate a given slip length. As the plate separation decreases the slip length generated by a given air gap thickness increases. At very

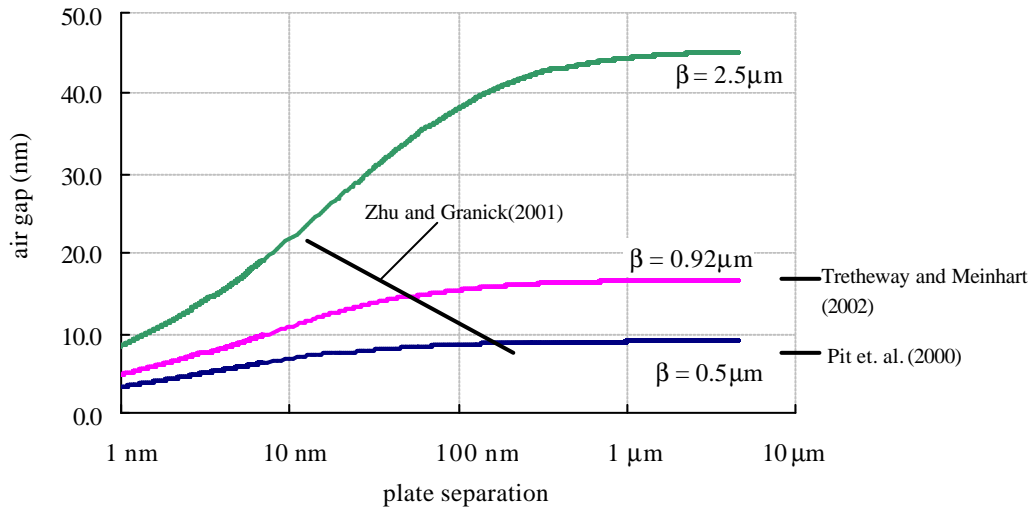


Figure 5. Solutions of Eq. (4), showing air gap thickness as a function of plate separation to produce a given slip length. Measured slip lengths for various researchers are indicated. Tyrell and Attard (2001) measured bubble heights of 20-30 nm.

small separations the slip length is strongly dependent on the air gap thickness. In this work we calculate a slip length of $0.92\ \mu\text{m}$. With $30\ \mu\text{m}$ channels, this yields a required air gap thickness of approximately 18nm . This thickness is consistent with the measured bubble heights of Tyrrell and Attard (2001). In addition, when surfaces are hydrophobic, Zhu and Granick (2001) calculated slip lengths of approximately $2.5\ \mu\text{m}$ for a 20nm separation. The corresponding bubble height of $\sim 20\text{nm}$ is consistent with the required bubble height in this work and the measured values of Tyrrell and Attard (2002). Pit et. al. (2000) calculate a slip length of approximately 400nm for a $190\ \mu\text{m}$ separation, which would require a bubble height of 9nm . These results suggest that the measured apparent fluid slip may develop as a result of dissolved or entrained gasses accumulating on hydrophobic surfaces. Current work with degassed water should elucidate the effects of soluble gasses.

While we calculate a slip length equal to $0.92\ \mu\text{m}$, the range of flow rates and thus shear rates in this work is limited. As a result, we are unable to make a conclusion with regards to Navier's hypothesis. Pit et. al. (2000) measure slip lengths that are independent of shear rate up to 2000s^{-1} . Zhu and Granick (2001) observe a critical shear rate for the onset of fluid slip, while Craig et. al. (2001) observe a non-linear dependence of the slip length on the driving rate. As a result of these discrepancies, it's not apparent that Navier's hypothesis is valid or not. Current work with a wider range of flow rates is being conducted to validate Navier's hypothesis.

5. Conclusions

In this work, we measure velocities within 450nm of hydrophilic and hydrophobic microchannel walls by micron resolution particle image velocimetry. For water flowing over a hydrophobic surface, a significant slip velocity at the wall is measured and a slip length of 0.92 microns is estimated. For a hydrophilic surface the no-slip boundary condition remains valid at the 30 micron lengthscale of the microchannel. A one dimensional air gap model for nano-bubbles at a surface predicts bubble heights of approximately 18nm , which is consistent with the measured bubble heights of Tyrrell and Attard (2001) and similar to the bubble heights required to produce the slip lengths of Zhu and Granick (2001) and Pit et. al. (2000). This indicates that the apparent fluid slip at a hydrophobic wall may result from the presence of nano-bubbles at the surface. Finally, the measured slip indicates that the no-slip boundary condition is not necessarily valid for flow of a hydrophilic liquid over a hydrophobic surface. Thus, modeling fluid flow at the micro-scale with the assumption of no-slip may or may not be accurate, but will depend on the interactions between the fluid and the surface properties of the wall.

Acknowledgements: This work is supported by NSF CTS-9874839, NSF ACI-0086061, and DARPA/Air Force 30602-00-2-0609.

References

- Barrat, J. and L. Bocquet "Large Elip Effect at a Nonwetting Fluid-Solid Interface". *Phys. Rev. Lett.*, **82**, 4671-4674 (1999).
- Churaev, N., V. Sobolev, and A. Somov "Slippage of Liquids Over Lyophobic Solid Surfaces". *J. of Colloid and Interface Science*, **97**, 574-581 (1984).
- Meinhart, C., S. Wereley, and J. Santiago "A PIV Algorithm for Estimating Time-Averaged Velocity Fields". *J. of Fluids Engineering*, **122**, 285-289 (2000).
- Navier, C. L. M. H., *Memoirs de l'Academie Royale des Sciences de l'Institut de France*, **1**, 414-416 (1823).
- Pit, R., H. Hervet, and L. Leger "Direct Experimental Evidence of Slip in Hexadecane: Solid Interfaces". *Phys. Rev. Lett.*, **85**, 980-983 (2000).
- Ruckenstein, E. and P. Rajora "On the No-Slip Boundary Condition of Hydrodynamics". *J. of Colloid and Interface Science*, **96**, 488-491 (1983).
- Tretheway, D. and C. Meinhart "Apparent Fluid Slip at Hydrophobic Microchannel Walls". *Physics of Fluids*, **14**, L9-L12 (2002).
- Tyrrell, J. and P. Attard "Images of Nanobubbles on Hydrophobic Surfaces and Their Interactions" *Phys. Rev. Lett.* **87**, 176104/1-4 (2001).
- Watanabe, K., Yanuar, and H. Mizunuma "Slip of Newtonian Fluids at Slid Boundary". *JSME International Journal Series B*, **41**, 525-529 (1998).

Watanabe, K., Yanuar, and H. Udagawa "Drag Reduction of Newtonian Fluid in a Circular Pipe With a Highly Water-Repellant Wall". J. of Fluid Mechanics, **381**, 225-238 (1999).

Zhu, Y. and S. Granick "Rate-dependent slip of Newtonian fluids at smooth surfaces". Phys. Rev. Lett. **87**, 96 (2001).